The Retroflection Paradox

DORON NOF AND THIERRY PICHEVIN*,+

Department of Oceanography and Geophysical Fluid Dynamics Institute, The Florida State University, Tallahassee, Florida

(Manuscript received 28 March 1995, in final form 4 August 1995)

ABSTRACT

The classical question of what happens when a warm western boundary current, such as the North Brazil Current (NBC), retroflects is addressed analytically using a reduced-gravity nonlinear model. The traditional view is that the northwestward flowing current separates from the wall, turns to the right (looking offshore), and forms a zonal boundary current that flows eastward. Integration of the steady inviscid momentum equation along the boundary gives the longshore momentum flux (or flow force) and shows that such a scenario leads to a paradox. To resolve the paradox the separated current must constantly shed anticyclones, which propagate to the northwest due to β and an interaction with the boundary. This new eddy shedding mechanism, which is not related to the traditional instability of a zonal jet, may explain why the NBC must produce rings.

A nonlinear analytical solution to the problem is constructed with the aid of a powerful theoretical approach based on the idea that *nonlinear periodic flows* can be integrated over a control volume. This method enables us to extract all the details of the resulting features without solving for the details of the incredibly complicated three-dimensional and time-dependent generation process. Due to the strong nonlinearity of the problem, the method is quite different from the familiar averaging technique that requires the existence of a "mean" current. To employ the above method, however, it was necessary to derive a new nonlinear formula for the β-induced migration of eddies adjacent to a zonal boundary that slopes in the N–S direction.

It turns out that the general problem involves an *eddy retroflection length scale* $R_d/\epsilon^{1/6}$ (where R_d is the parent current Rossby radius and $\epsilon = \beta R_d/f_0$) that is *greater* than that of most eddies (R_d). Calculations show that, for the retroflected NBC, which transports about 45 Sv, eddies are shed approximately once every 90 days.

1. Introduction

The question of how and why retroflection eddies are generated is important for our understanding of the transfer of mass, salt, and heat. Traditionally, eddy formation processes have been associated with classical instabilities of zonal currents and fronts.[1] Such zonal instabilities generate meanders that grow, close upon themselves, and then pinch off. Although this is probably the correct formation mechanism for many eddies and rings in the ocean (e.g., Gulf Stream and Kuroshio rings), retroflection eddies are always generated in the same location, suggesting some other, geographically controlled, formation mechanism. This suggestion is supported by the observations that retroflection rings are typically larger than rings produced by classical instability of zonal currents (e.g., see Richardson et al. 1994).

This paper focuses on a new eddy generation process that is associated with such a geographical control and a larger length scale. Specifically, we focus on western boundary currents, such as the North Brazil Current (NBC), which turn backward away from their original direction due to a separation from the wall. We shall see that a retroflection of this kind *leads to a paradox* because it produces an unbalanced flow force. This force can only be compensated for by shedding eddies in the currents' original direction. The present article has two goals. The first is to explain why NBC rings are formed and the second is to propose an explanation for their relatively small migration rate.

a. Observational background

The suggestion that the western tropical Atlantic is important to the meridional heat flux comes from the observation that at subtropical latitudes western boundary currents represent an important component of the global heat budget (Bryden and Hall 1980). Observations imply that, at the surface, the summer and fall circulation in the western tropical Atlantic is dominated by the retroflection of the NBC, which carries up to 50 Sv (Sv $\equiv 10^6$ m^3 s^{-1}) of surface water to the east

[1] Note that by "instability" we mean here the instability of a zonal jet such as the separated Gulf Stream; we do not refer to all time-dependent processes as "instabilities."

* Additional affiliation: LODYC, Université Pierre et Marie Curie, Paris, France

+ On leave from: SHOM/CMO, Brest, France

Corresponding author address: Prof. Doron Nof, Department of Oceanography 3048, The Florida State University, Tallahassee, FL 32306-3048

E-mail: nof@ocean.fsu.edu.

© 1996 American Meteorological Society

(Brown et al. 1992). The water immediately below the thermocline also retroflects (Metcalf and Stalcup 1967) but, evidently, this occurs at a different latitude. During other periods of the year (i.e., winter and spring) the NBC does not retroflect.

The observations of Johns et al. (1990), Didden and Schott (1993), Richardson et al. (1994), and Fratantoni et al. (1995) all suggest that the NBC retroflection sheds two or three eddies per year. Through the eddy migration, about 3–4 Sv [20% of the total upper-ocean cross-gyre transport required by Atlantic thermohaline overturning (Rintoul 1991)] is annually transported to the North Atlantic. As is the case with most rings resulting from retroflecting currents, NBC rings are larger than rings such as Gulf Stream or Kuroshio rings. They have a diameter of roughly 400–600 km and a depth of 400–600 m; they migrate at a rate of 10–12 cm s^{-1} along the coast (Fig. 1). As mentioned, the large size of these rings and that the rings are always formed at the same location suggest that, in contrast to many rings, they are probably not formed by an instability process. Instead, their generation is probably a result of the particular structure of the current, which loops and curves back on itself. For other issues related to these rings the reader is referred to Bruce and Kerling (1984), Bruce (1984), Bruce et al. (1985), and Cochrane et al. (1979).

b. Theoretical background

The dynamics of the western tropical Atlantic and the NBC retroflection region were examined analytically by Csanady (1985, 1990) and Condie (1991) using steady inertial models. Although a portion of the NBC water leaks to the north along the coast in some of these models, the leakage is steady and, as such, it does not explain how and why NBC rings are generated. Also, both the high-resolution numerical models used by Philander and Pacanowski (1986) (i.e., the GFDL Tropical Atlantic Model) and the NCAR Community Model (Holland and Bryan 1987; Schott and Boning 1991) do not produce NBC rings (Fratantoni et al. 1995; Johns et al. 1990; Didden and Schott 1993). In contrast, a modification of the Navy Ocean Model [originally developed for the Gulf of Mexico by Hurlburt and Thompson (1980)] does exhibit NBC rings (Fratantoni et al. 1995). Why this is so is not clear. Ou and De Ruijter (1986) suggest that Agulhas retroflection rings are produced due to curvature constraints. Although their model is useful and may shed some light on the separation process, it does not provide information regarding the eddies' generation frequency.

c. Present approach

We shall model the eddy generation process as follows. First, we shall consider a northwestward flowing boundary current (with density ρ) embedded in an infinitely deep lower layer [with a density $(\rho + \Delta\rho)$]. It is assumed that the current turns eastward (Fig. 2a) after separating from the wall. The cause of the separation is a vanishing wind stress curl over the ocean interior. We shall show in section 2 that, even though the above scenario of a steady current that turns back

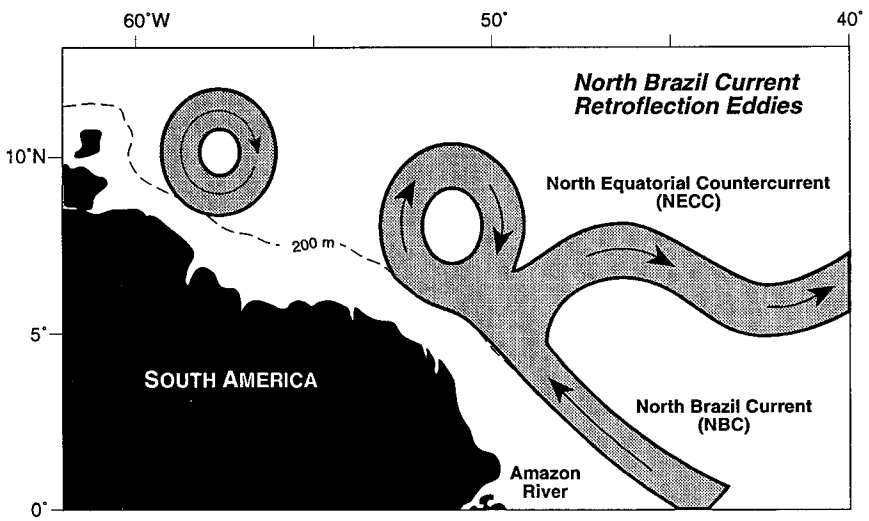

FIG. 1. Schematic diagram showing the formation of a North Brazil Current (NBC) retroflection eddy based on images shown by Johns et al. (1990). Three to four times each year starting in July the NBC retroflection advances northwestward along the boundary to about 9°–10°N forming a current loop. The sides of the loop come together, and the current loop pinches off from the main current to form a discrete eddy. As the eddy separates, the retroflection forms farther south near 5°–6°N. Retroflection eddies are about 400 km in overall diameter and drift northwestward at about 10–12 cm s^{-1}. Adapted from Richardson et al. (1994).

on itself seems reasonable, it cannot exist. This is so because the westward flow force associated with the water entering and leaving the box (bounded by the dashed line shown in Fig. 2a) cannot be balanced.

A similar paradox exists in the case of a channel emptying into an otherwise stagnant ocean and was referred to by Pichevin and Nof (1996a, hereafter PNa) as "the momentum imbalance paradox." It also exists in the case of a flow around a cape (Pichevin and Nof 1996b, hereafter PNb). A resolution of the paradox requires the generation of eddies that would leave the box on the left-hand side (looking northward). Under such conditions, the eddies compensate for the flow-force exerted on the box by the flow on the right-hand side. This is shown in section 3 using a computational method [used earlier by PNa,b] that involves analytical integration of periodic flows over the box (Fig. 2a).

A perturbation scheme in a small parameter representing the ratio between the eddy drift speed and the current speed is then applied to simplify the resulting algebraic equations (sections 4 and 5). There is some (unavoidable) overlap between the theoretical development of the present paper and that presented in PNa,b because an attempt has been made to make the present paper self-contained. The application is discussed in detail in sections 4 and 5, where it is shown that β alone (i.e., no bottom topography) would produce NBC rings at a frequency that is considerably greater than the observed frequency (a few NBC rings a year). As mentioned, this is because β alone produces a migration rate considerably higher than the observed rate. The presence of bottom topography or an eastward advection, however, reduces the generation frequency to an acceptable level. We believe that the presence of bottom topography is essential and derive a new formula for the propagation of eddies adjacent to zonal walls with sloping bottom (section 6). Our formula illustrates that, in the case of the NBC, the sloping topography reduces the westward propagation rate and therefore the generation frequency.

The article is organized as follows. The details of the new eddy generation process are described in section 2 where the problem is formulated. The mathematical technique is described in sections 3 and 4, and the solution for zero and uniform potential vorticity flows is given in section 5. The effects of topography are analyzed in section 6. The conclusions are given in section 7.

2. Formulation

This section describes the physics of the problem and the mathematical approach.

a. The paradox

We suggest that NBC rings are generated by a new and intriguing process that is a result of the momentum imbalance paradox discussed by PNa,b. The principle of this imbalance as it applies to the NBC is best illustrated as follows.

Consider a northwestward boundary current carrying relatively light water (with density ρ) retroflecting into an otherwise stagnant ocean (with density $\rho + \Delta\rho$) and flowing eastward (Fig. 2a). The cause of the retroflection is not important for our analysis, but one may consider it to be a result of vanishing wind stress over the interior. If one (temporarily) assumes that a steady state is reached, then one can integrate the steady nonlinear x momentum equation over the region (S) bounded by the dashed line ABCDEFG shown in Fig. 2a,

$$\iint_S \left[hu\frac{\partial u}{\partial x} + hv\frac{\partial u}{\partial y} - fvh + g'h\frac{\partial h}{\partial x}\right] dxdy = 0, \tag{2.1}$$

where, due to the tilt of our coordinate system $f = f_0 + \beta(y\cos\gamma - x\sin\gamma)$, h is the thickness of the light water, S is the integration area, and the remaining notation is conventional. (Note that, for convenience, the variables are defined both in the text and the appendix.)

Using the continuity equation and a streamfunction ψ (defined by $\partial\psi/\partial x = vh$; $\partial\psi/\partial y = -uh$), (2.1) can also be written as

$$\iint_S \left[\frac{\partial}{\partial x}(hu^2) + \frac{\partial}{\partial y}(huv)\right] dxdy - \iint_S f\frac{\partial\psi}{\partial x}dxdy + \frac{g'}{2}\iint_S \frac{\partial(h^2)}{\partial x}dxdy = 0. \tag{2.1a}$$

We shall now assume that the angle γ is small so that $\cos\gamma \approx 1$ and $\sin\gamma \approx 0$ (Fig. 2b) implying that $\partial(f\psi)/\partial x = f\partial\psi/\partial x$. It will become clear later that,

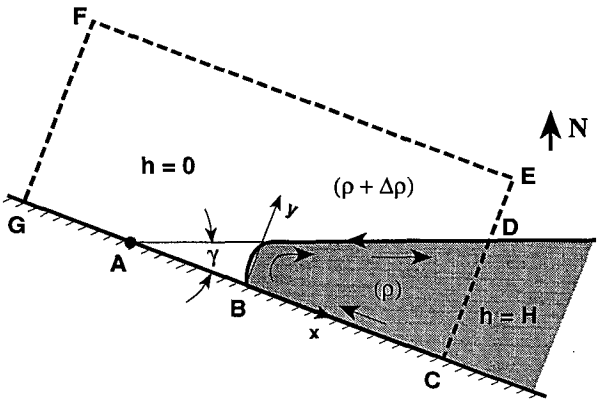

FIG. 2a. Schematic diagram of the retroflected NBC. The cause of the retroflection is not important for the present study, but one may assume that it results from a vanishing wind stress curl over the interior. The dashed line shows the boundary of the integration area; γ is the tilt of the coastline; H is the undisturbed depth away from the wall where the velocity vanishes.

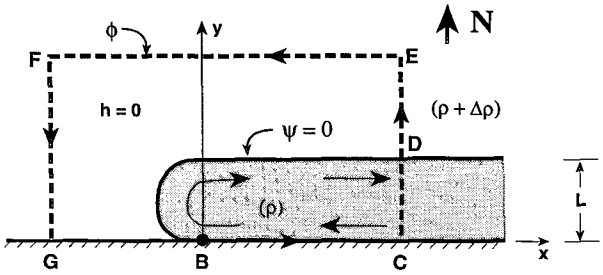

FIG. 2b. The approximated retroflection. Here, the tilt of the coastline shown in Fig. 2a is taken to be small and negligible (i.e., $\gamma = 0$). Consequently, the approaching and retroflecting currents are parallel to each other. It will become clear later that this small tilt approximation is consistent with our perturbation expansion as long as $\gamma \lesssim (\beta R_d/f_0)^{1/6}$. It is shown in the text that if the retroflection were steady, then integration of the x momentum equation over the region bounded by the dashed line would give a relationship that cannot be satisfied. This implies that, under such conditions, the flow force exerted by the currents in the direction parallel to the wall is not balanced. The only way that it can be balanced is by generating eddies that will propagate in the negative x direction due to β.

to the order of our approximation, this requires that $\gamma \lesssim (\beta R_d/f_0)^{1/6}$, where R_d is the Rossby radius. For our problem, $\beta R_d/f_0 \sim 0.2$ so that the coastline tilt of the South American continent ($\sim 30°$, see Fig. 1) can indeed be neglected (when γ is not small, there is an additional force that cannot be computed with our technique). With the aid of the Stokes theorem [i.e.,

$$\iint_S (\partial M/\partial x + \partial N/\partial y)dxdy = \oint Ndx - \oint Mdy,$$

where the arrowed circles represent counterclockwise integration], (2.1a) can now be simplified

$$\oint_{\mathrm{BCDEFGB}} huvdx - \oint_{\mathrm{BCDEFGB}} \times (hu^2 + g'h^2/2 - f\psi)dy = 0, \quad (2.1b)$$

where BCDEFGB is the boundary of S.

Defining $\psi = 0$ where $h = 0$, and noting that $v \equiv 0$ on the solid boundary, one finds that (2.1b) can also be written as

$$\int_C^D [hu^2 + g'h^2/2 - f\psi]dy = 0. \quad (2.2)$$

Noting further that since the flow is geostrophic in CD (so that $fu = -g'hy$, which, upon multiplication by h and integration in y from a point within the current to its edge, gives $f\psi = g'h^2/2 - \beta\int_y^L \psi dy$), relation (2.2) reduces to the simple relationship,

$$\boxed{\int_0^L hu^2dy + \beta\int_0^L\left(\int_y^L \psi dy\right)dy = 0,} \quad (2.3)$$

where L is the combined width of the approaching and retroflecting current.

The curious result is that condition (2.3) cannot be satisfied because y and ψ are always positive along CD and the integration is done from small to large y. For most boundary currents [i.e., $U \sim O(g'H)^{1/2}$; $L \sim O(g'H)^{1/2}/f$], the second term [$O(\beta L/f_0)$] is much smaller than the first term [$\sim O(1)$]. The impossibility of satisfying (2.3) implies that there cannot be a steady state of the kind originally assumed because the integrated momentum (i.e., momentum flux or flow-force) imparted (by the fluid entering and exiting through CD) on the control volume (bounded by BCDEFG) cannot be balanced. The only way that the retroflected flow field can balance this momentum flux is by somehow creating a flow in the opposite sense (i.e., the negative x direction). However, a light westward current with a finite cross section is impossible without a wall on the north side against which it can lean. As we shall see, this means that the balance can only be achieved via the generation of anticyclonic eddies, which propagate to the left due to β (Fig. 3). The computation of this situation is discussed in the following sections.

For clarity, it will be first assumed that the zonal wall is vertical so that bottom topography plays no role in the eddy migration. After presenting the result for this case we shall analyze the more realistic case where bottom topography is important (section 6).

b. *The unsteady integrated momentum theorem for a current adjacent to a vertical wall (i.e., no bottom topography)*

As mentioned, to solve for the size, number, and periodicity of the generated eddies we shall apply the integrated momentum theorem for periodic flows developed by PNa,b. This general equation will enable us to circumvent the time-dependent generation process itself. That is, this technique will give us all the

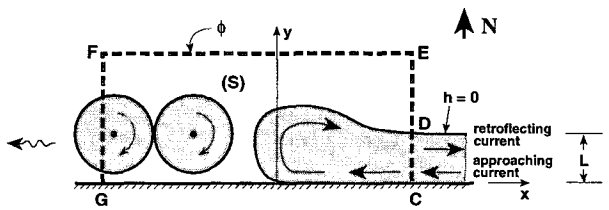

FIG. 3. The resolution of the retroflection paradox. Because of the imbalance shown in Fig. 2, anticyclonic eddies must be generated on the left-hand side (looking offshore). Through the β effect these eddies are forced to propagate to the left. Under such conditions the flow force exerted by the retroflected flow on the right is now balanced by the force corresponding to the eddies' transport to the left. We shall see that, even though the mass transport of the eddies is small compared to the transport of the approaching and retroflecting currents, the flow force of the drifting eddies is comparable to that of the currents. The "wiggly" arrow denotes migration and should be distinguished from solid arrows that denote flow direction. L is the combined width of the (known) approaching current and the (unknown) retroflecting current.

information that we need regarding the eddies exiting the domain and the outcome of the generation process without giving us information about the detailed formation process itself. [The reader who is not interested in the mathematical presentation and development which, because of space constraints, can be at times difficult to follow, can go directly to Eq. (2.9), which is our desired relationship.]

To derive the desired equation we begin with an integration of the time-dependent x momentum equation (multiplied by h) once in time,

$$\int_0^T h\frac{\partial u}{\partial t}dt + \int_0^T hu\frac{\partial u}{\partial x}dt + \int_0^T hv\frac{\partial u}{\partial y}dt - \int_0^T hfvdt = -\int_0^T g'\frac{\partial}{\partial x}(h^2/2)dt, \quad (2.4)$$

where T is the period of eddy generation and, since we took γ to be small, $f = f_0 + \beta y$.

Leaving (2.4) aside for a moment, we note that multiplication of the continuity equation by u and integration in time over one period gives

$$\int_0^T u\frac{\partial h}{\partial t}dt + \int_0^T u\frac{\partial}{\partial x}(hu)dt + \int_0^T u\frac{\partial}{\partial y}(hv)dt = 0.$$

Adding this equation to (2.4) gives

$$\int_0^T \frac{\partial}{\partial x}(hu^2)dt + \int_0^T \frac{\partial}{\partial y}(huv)dt - \int_0^T hfvdt + \int_0^T \frac{g'}{2}\frac{\partial}{\partial x}(h^2)dt = 0, \quad (2.4a)$$

because

$$\int_0^T \frac{\partial}{\partial t}(hu)dt = hu|_T - hu|_0 = 0$$

(i.e., the system always returns to its original structure after one generation period). We now integrate (2.4a) over S (Fig. 3). Since the domain S is fixed, we can exchange the order of integration with respect to time and space. One finds

$$\int_0^T \iint_S \frac{\partial}{\partial x}(hu^2)dxdydt + \int_0^T \iint_S \frac{\partial}{\partial y}(huv)dxdydt - \int_0^T \iint_S hfvdxdydt + \frac{g'}{2}\int_0^T \iint_S \frac{\partial}{\partial x}\left(\frac{h^2}{2}\right)dxdydt = 0. \quad (2.5)$$

Next, we define a time-integrated streamfunction $\tilde{\psi}$ (to be distinguished from the steady streamfunction ψ, which is defined in the usual manner),

$$\left.\begin{aligned}\tilde{\psi}_y &= -\int_0^T hudt\\ \tilde{\psi}_x &= \int_0^T hvdt\end{aligned}\right\}. \quad (2.6)$$

This definition stems from an integration of the continuity equation in time (from zero to T), noting again that $h(T) = h(0)$ and changing the order of integration so that

$$\frac{\partial}{\partial x}\left(\int_0^T hudt\right) + \frac{\partial}{\partial y}\left(\int_0^T hvdt\right) = 0. \quad (2.7)$$

The streamfunction and Stokes theorem (and that along the zonal boundary at least one of the three variables h, u, and v is always zero) enable us to express (2.5) as

$$\int_0^T \oint_\phi hu^2dydt - \oint_\phi f\tilde{\psi}dy + \frac{g'}{2}\oint_\phi \int_0^T h^2dydt = 0, \quad (2.8)$$

where the arrowed circle denotes counterclockwise integration and ϕ is the boundary of the integration area S.

Assuming that the flow away from the eddy generation region across CD (Fig. 3) is steady, (2.8) can also be written as

$$\boxed{\int_0^T \int_G^F (hu^2 + g'h^2/2)dydt - \int_G^F f\tilde{\psi}dy = T\int_C^D (hu^2 - f\psi + g'h^2/2)dy,} \quad (2.9)$$

where, as before, ψ is the steady streamfunction defined in the usual manner.

Equation (2.9) is our desired *flow-force balance.* In an analogy to a rocket and a spinning sprinkler, the right-hand side corresponds to the flow force exerted on the domain by the water entering and exiting on the right. It is the flow force (or integrated momentum) that we argued is not balanced unless eddies are shed on the left. The term on the left-hand side of (2.9) corresponds to the flow force exerted by the eddies moving to the left out of the domain. In this context, it is important to point out that the role of β in our problem is to arrest the growth of the eddies and remove them from the generation area. It is a simple matter to compute the contribution of the steady current on the right to (2.9) but computation of eddies contribution (which is time dependent) is not so trivial. It is, therefore, discussed in detail in the next section.

c. Other constraints

In addition to the above momentum constraint, the field must, of course, satisfy the continuity equation,

$$-\int_C^D hudy + \frac{1}{T}\iint_{\text{eddy}} hdxdy = 0, \qquad (2.10)$$

and the conservation of potential vorticity equation,

$$\frac{D}{Dt}\left(\frac{\partial v/\partial x - \partial h/\partial y + f}{h}\right) \equiv 0. \qquad (2.11)$$

We shall see that the above system of equations (2.9)–(2.11) enables us to close the problem provided that we assume that the resulting eddies are in contact with each other as they leave the domain. (This does not mean that, during the formation process, the current is always in contact with the separated ring. All it says is that the eddies touch each other when they leave the generation area.) Since the approaching current is known and the β-induced eddy drift is also known (e.g., see Nof 1981), Eq. (2.9) involves two unknowns (the retroflected current transport and the eddy size). The solution for these two unknowns will be provided by (2.10) and (2.11).

3. The integrated momentum balance for vertical walls (no bottom topography)

As mentioned, this calculation is not straightforward because all terms associated with the left-hand side of Eq. (2.9) are time dependent. To simplify the procedure, we shall transform those terms to a new coordinate system $(\hat{x}, \hat{y}, \hat{t})$ moving steadily westward at the speed of the eddies (Fig. 4).

a. Transformation to a moving coordinate system

The relationship between the fixed system (x, y, t) and the new moving system $(\hat{x}, \hat{y}, \hat{t})$ is

$$t = \hat{t}; \quad x = \hat{x} + C\hat{t}; \quad y = \hat{y}, \qquad (3.1)$$

where C is the migration rate (taken to be positive when it is directed in the positive x direction). According to (3.1), the transformed integrations are associated with

$$dt = d\hat{t} \qquad (3.2a)$$

$$dy = d\hat{y} \qquad (3.2b)$$

$$dx = d\hat{x} + Cd\hat{t}. \qquad (3.2c)$$

Since the integration in time is done holding x fixed, (3.2c) shows that it can be done using the relationship $d\hat{x} = -Cd\hat{t}$, which implies

$$d\hat{t} = -\frac{1}{C}d\hat{x}. \qquad (3.3)$$

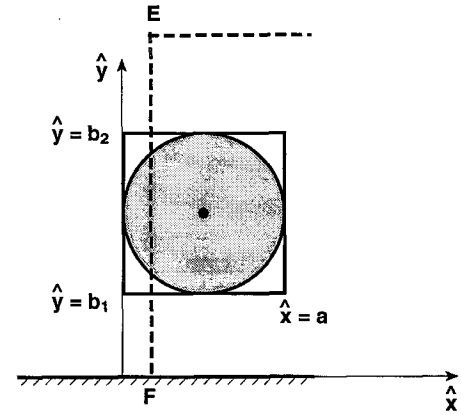

FIG. 4. Schematic diagram of the eddy's integration area in the moving coordinate system $(\hat{x}, \hat{y}, \hat{t})$. The integration is done over the square bounded by $\hat{x} = 0$; $\hat{x} = a$ and $\hat{y} = b_1$; $\hat{y} = b_2$, that is, a bounding rectangle that touches the eddy. The dashed line denotes the fixed integration boundary through which the eddy is exiting (see Fig. 3).

In view of this, the left-hand side of (2.9), which describes the exit of the eddy, takes the form

$$-\frac{1}{C}\int_0^a\int_{b_1}^{b_2} h(\hat{u} + C)^2 d\hat{y}d\hat{x} - \int_{b_1}^{b_2} f\tilde{\psi}d\hat{y} - \frac{g'}{2C}\int_0^a\int_{b_1}^{b_2} h^2 d\hat{y}d\hat{x}, \qquad (3.4)$$

where

$$\frac{\partial\tilde{\psi}}{\partial\hat{y}} = \frac{1}{C}\int_0^a h(\hat{u} + C)d\hat{x} = -\frac{1}{C}\int_0^a \frac{\partial\hat{\psi}}{\partial\hat{y}}d\hat{x} + \int_0^a hd\hat{x}. \qquad (3.5)$$

Relation (3.5) can be integrated in $\hat{y}$ to give

$$\tilde{\psi}(b_2) - \tilde{\psi}(\hat{y}) = \frac{1}{C}\int_0^a \hat{\psi}d\hat{x} + \int_{\hat{y}}^{b_2}\int_0^a hd\hat{x}d\hat{y}, \qquad (3.5a)$$

where we defined $\hat{\psi}$ to be zero outside the eddy. Also, without loss of generality, we can choose $\tilde{\psi}(b_2) = 0$; if this choice is not made, the terms involving $\tilde{\psi}(b_2)$ will ultimately drop out anyway. Note that the integration described by (3.4) is done over a bounding rectangle that touches the eddy (Fig. 4). Also note that here $\tilde{\psi}$ is the *time-integrated streamfunction,* which is different from both the streamfunction in the moving system $\hat{\psi}$ [originating from the continuity equation $\partial(h\hat{u})/\partial\hat{x} + \partial(h\hat{v})/\partial\hat{y} = 0$] and the usual streamfunction ψ.

b. Simplifications

Although the computation of (3.4) is easier than that of the original left-hand side of (2.9) (because it is no longer time dependent) it is still not so simple. We shall now show that (3.4) can be simplified to

$$-\int_0^a \int_{b_1}^{b_2} hC d\hat{y} d\hat{x} + \int_{b_1}^{b_2} f \left[\int_{\hat{y}}^{b_2} \left(\int_0^a h d\hat{x} \right) d\hat{y} \right] d\hat{y}. \quad (3.6)$$

To show this we note that integration of the transformed $\hat{x}$ momentum equation over part of the eddy bounded by $h = 0$ on the west and a meridional line on the east gives

$$\iint \left\{ \frac{\partial}{\partial \hat{x}} (h\hat{u}^2) + \frac{\partial}{\partial \hat{y}} (h\hat{u}\hat{v}) - f\hat{v}h + \frac{g'}{2} \frac{\partial}{\partial \hat{x}} (h^2) \right\} d\hat{x} d\hat{y} = 0. \quad (3.7)$$

The use of Stokes theorem and that $h = 0$ and $\hat{\psi} = 0$ outside the eddy shows that for any $\hat{x}$

$$\int_{b_1}^{b_2} (h\hat{u}^2 + g'h^2/2 - f\hat{\psi}) d\hat{y} = 0.$$

This, together with the condition $\iint h\hat{u} d\hat{x} d\hat{y} = 0$ (resulting from $\oint \hat{\psi} d\hat{x} = 0$), completes our demonstration that (3.4) can be replaced by (3.6).

c. *The resulting equation*

To evaluate the right-hand side of (2.9), we will need to compute the term $(g'h^2/2 - f\psi)$. To do so, we note that $\psi = \tilde{\psi}/T = 0$ along the steady current edge ($y = L$) because there is no mass flux in between the eddy and the current edge where $h \equiv 0$ (i.e., $\tilde{\psi} = 0$ everywhere outside the eddy and the current). Since the flow is geostrophic across CD, it follows that $g'h^2/2 = f\psi - \beta \int_L^y \psi dy$. Using this condition and substituting (3.6) into the left-hand side of (2.9) gives the desired relationship:

$$-C \int_{b_1}^{b_2} \int_0^a h d\hat{x} d\hat{y} + \underbrace{\int_{b_1}^{b_2} \left[f \int_{\hat{y}}^{b_2} \left(\int_0^a h d\hat{x} \right) d\hat{y} \right] d\hat{y}}_{\mathrm{I}}$$

$$= \underbrace{T \int_0^L hu^2 dy}_{\mathrm{II}} + \beta T \int_0^L \int_y^L \psi dy dy. \quad (3.8)$$

As mentioned, the left-hand side of (3.8) corresponds to the momentum flux (or flow force) exerted on the region by the exiting eddies, whereas the right-hand side is associated with the momentum flux of the steady approaching and retroflecting currents. By noting that the eddy migration rate is $O(\beta R_{de}^2)$ so that $C/\beta R_{de} \sim O(\beta R_{de}/f_0) \ll 1$, and $\beta R_d/f_0 \ll 1$ (where R_{de} and R_d are the eddy and approaching current Rossby radii), it is a simple matter to show that the dominant terms in (3.8) are I and II.

Three comments should be made with regard to (3.8). First, it is important to realize that, even though (3.8) represents a balance of momentum flux integrated over a period T, the time-dependent momentum flux varies as each eddy passes (through the western boundary) leaving an instantaneous and periodic imbalance. This means that the retroflection part of the flow also cannot be steady. It must advance and retreat into the control volume in accordance with the eddy formation process. A similar aspect can be noted in the observations of Richardson et al. (1994). Second, it is important to realize that not all situations corresponding to (3.8) are associated with the generation of eddies because, in the absence of an eddy removal mechanism (e.g., $\beta \equiv 0$), the flow may not be periodic but rather may evolve constantly in time. Third, (3.8) does not necessarily imply that the eddies are in contact with each other as they leave the control volume. Spacing between the eddies is clearly possible, but one has to make a choice about the exiting eddies in order to close the problem. It is difficult to say where the edge of actual eddies in the ocean is but the choice of touching eddies appears to be in reasonable agreement with observations (Richardson et al. 1994). Even if it were not in good agreement, it would have still been useful because it provides an *upper bound* on the generation frequency and eddy size.

4. Scaling and expansion for the no bottom topography case

a. *Scales*

Since the eddies are slowly removed from the generation area by β (at a speed of the order of βR_{de}^2), one expects their length scale to be much greater than the current's length scale. Indeed, a comparison of the second term on the left and the first term on the right of (3.8) (i.e., the largest terms on each side) gives

$$fH_e R_{de}^3 \sim O\left[\frac{R_{de}}{\beta R_{de}^2} H(g'H) R_d \right],$$

which yields

$$R_{de} \sim O(R_d/\epsilon^{1/6}), \quad (4.1)$$

where $\epsilon \equiv \beta R_d/f_0 \ll 1$, and it has been assumed that the eddies moving out of the area are not far from each other [i.e., $T \sim O(a/C)$]. (As mentioned, we shall later consider eddies that are in contact with each other as they leave the control box, but it is not necessary to make this choice at this stage.) Note that in obtaining (4.1) it has been taken into account that the ratio of the eddy depth scale H_e and the approaching current depth scale H is given by R_{de}^2/R_d^2. In view of (4.1), the periodicity at which the eddies are generated (T) is

$$T \sim O(\epsilon^{1/6}/\beta R_d). \tag{4.2}$$

These scales are sensible for the NBC as the parameter ϵ is $\sim O(0.1)$ implying that the eddies are somewhat larger than most rings; the eddy depth scale h_e is of the order of the current depth divided by $\epsilon^{1/3}$.

Given the above scales, we now introduce the following nondimensional parameters. For the currents entering and leaving the control volume through CD the scaled variables are

$$x^* = x/R_d; \quad y^* = y/R_d;$$
$$v^* = v/(g'H)^{1/2}; \quad h^* = h/H;$$
$$R_d \equiv (g'H)^{1/2}/f_0; \quad \psi^* = \psi/g'H^2/f_0; \tag{4.3}$$

where H is the upstream undisturbed depth (i.e., the depth away from the wall where the velocity vanishes). Similarly, the scaled variables for the eddies are

$$x_e^* = x/R_{de}; \quad y_e^* = y/R_{de}; \quad h_e^* = \frac{h}{H\left(\frac{R_{de}}{R_d}\right)^2}$$
$$C^* = C/\beta R_{de}^2; \quad R_{de} = \alpha R_d/\epsilon^{1/6}; \quad \alpha \sim O(1)$$
$$\epsilon \equiv \beta R_d/f_0 \ll 1; \quad T^* = \frac{T}{\epsilon^{1/6}/\beta R_d}; \tag{4.4}$$

where α is an unknown number of order unity that measures the size of the resulting eddies and the subscript "e" indicates association with the eddies. Note that the introduction of α in (4.4) is necessary because the Rossby radius of the eddies determines their size and speed and that the above scaling is the only one that satisfies both the momentum and mass balance.

b. *The nondimensional equations*

Substitution of (4.3) and (4.4) into the integrated momentum (3.8) gives

$$C^*\alpha^5\epsilon^{5/6}\int_{b_1^*}^{b_2^*}\int_0^{a^*} h_e^* dx_e^* dy_e^* + \alpha^5\int_{b_1^*}^{b_2^*}(1+\alpha\epsilon^{5/6}y_e^*)\int_{y^*}^{b_2^*}\left(\int_0^{a^*} h_e^* dx_e^*\right)dy_e^* dy_e^*$$
$$= T^*\int_0^{L^*} h^*(u^*)^2 dy^* + \epsilon T^*\int_0^{L^*}\int_{y^*}^{L^*}\psi^* dy^* dy^*. \tag{4.5}$$

Similarly, the continuity equation can be written as

$$\int_0^{L^*} h^* u^* dy^* + \frac{\alpha^4\epsilon^{1/6}}{T^*}\int_0^{a^*}\int_{b_1^*}^{b_2^*} h_e^* dy_e^* dx_e^* = 0. \tag{4.6}$$

Recall that, in addition to the above two equations, the field is governed by the potential vorticity equation (2.11). We shall shortly see that this, together with the assumption that the eddies are in contact with each other as they leave [which, as mentioned, is in reasonable agreement with the observations of Richardson et al. (1994)] and that we know the eddy migration rate on a β plane, will enable us to close the problem. Note that the problem is subject to any additional constraints and that the frequently used Bernoulli integral cannot be applied to the edge of the current ($h = 0$) because our flow is *unsteady.*

c. *Expansions*

To obtain the solution, all dependent variables are now expanded in a power series in $\epsilon^{1/6}$; for example,

$$\left.\begin{aligned} h_e^* &= h_e^{(0)} + \epsilon^{1/6}h_e^{(1)} + \cdots \\ h^* &= h^{(0)} + \epsilon^{1/6}h^{(1)} + \cdots \\ u^* &= u^{(0)} + \epsilon^{1/6}u^{(1)} + \cdots \end{aligned}\right\}. \tag{4.7}$$

Substitution of (4.7) into (4.5) and (4.6) gives the following leading-order balances:

$$\int_{b_1^{(0)}}^{b_2^{(0)}}\int_{y_e^*}^{b_2^{(0)}}\left(\int_0^{a^{(0)}} h_e^{(0)} dx_e^*\right)dy_e^* dy_e^*$$
$$= \frac{T^{(0)}}{(\alpha^{(0)})^5}\int_0^{L^{(0)}} h^{(0)}(u^{(0)})^2 dy^* \tag{4.8}$$
$$\int_0^{L^{(0)}} h^{(0)}u^{(0)} dy_e^* = 0. \tag{4.9}$$

These balances imply that the mass removed by the eddies is small and negligible (to leading order ϵ^0), but the *momentum* exerted by the translating eddies is not small and *cannot be neglected.* The periodicity $T^{(0)}$ is related to the eddy β-induced drift through the diameter of the eddies.

5. Solution for the no bottom topography case

Since our scaling implies that the eddies must be much deeper than the parent current [$H_e \sim O(H/\epsilon^{1/3})$], it follows that the parent current must have strong anticyclonic vorticity. This results from conservation of potential vorticity. It implies that the eddy vorticity will be anticyclonic (despite the severe stretching of the water column that occurs during the formation) only if the parent current vorticity is strongly anticyclonic. The NBC satisfies this condition of strong anticyclonic vorticity; observations suggest that its potential vorticity is close to zero (e.g., see Csanady 1985). What would

happen when the parent current vorticity is not strongly anticyclonic is not entirely clear. The three eddy-generation cases that we have examined [i.e., the presently discussed NBC, the Mediterranean outflow (PNb) and the Gulf of Mexico (PNa)] have parent currents with strong anticyclonic shear as required.

a. Zero potential vorticity eddies

We shall first examine the case where both the current and rings have zero potential vorticity. For this case, the solutions for both the current and the eddies are straightforward despite the nonlinearity. Specifically, the leading-order solution for the approaching and retroflecting current is

$$\left.\begin{aligned} u &= f_0\left(y - \frac{L}{2}\right) \\ h &= -\frac{f_0^2}{2g'}(y^2 - Ly) \end{aligned}\right\}, \tag{5.1}$$

where L is the (combined) current width given by

$$L = 2(2g'H)^{1/2}/f_0, \tag{5.2}$$

and we have already taken (4.9) into account in the sense that we forced the flux of the retroflected current to be equal to that of the approaching current.

Similarly, the leading-order solution for the eddy is

$$\left.\begin{aligned} v_\theta &= -fr/2 \\ h &= \frac{f_0^2}{8g'}(8R_{de}^2 - r^2) \end{aligned}\right\}, \tag{5.3}$$

where, for simplicity, we use here a polar coordinate system (r, θ) whose origin coincides with the center of the eddy; R_{de} is the (unknown) Rossby radius of the eddy. Substitution of (5.1), (5.2), and (5.3) into (4.8) gives one equation with *one* unknown, the eddy size (R), which is related to its Rossby radius R_{de}.

One finds

$$\boxed{\alpha = \frac{2^{1/4}}{(5\pi)^{1/6}}}\,;\quad \boxed{T = \frac{24(5\pi)^{1/6}}{2^{7/4} f \epsilon^{5/6}}}\,;\quad \boxed{R = \frac{2^{7/4}}{(5\pi)^{1/6}}\frac{R_d}{\epsilon^{1/6}}}.$$

In deriving the solution, it has been taken into account that the westward migration of a zero potential vorticity eddy due to β is $-\frac{2}{3}\beta R_{de}^2$ (see Nof 1981).

b. Finite potential vorticity eddies

We shall now look at the case where the parent current potential vorticity is still zero (or very close to zero) but the eddy (uniform) potential vorticity is nonzero and finite. This case is a bit confusing but, to $O(\epsilon^{1/6})$, is consistent with both our scaling and conservation of potential vorticity. To see this, recall that

$$\frac{\xi_e + f}{h_e} = \frac{\xi + f}{h} = \frac{f}{H_p},$$

where ξ and ξ_e are the relative vorticities of the current and eddy, h and h_e are their depths, and H_p is the "potential vorticity depth" of both the current and the eddies. We now note that, according to our scaling, $h \sim O(\epsilon^{1/3}H_p)$ and $h_e \sim O(H_p)$. This means that even though the eddies may have uniform and finite potential vorticity $[h_e \sim O(H_p)]$ the current effectively [i.e., to $O(\epsilon^{1/6})$] has zero potential vorticity because its depth (h) is much smaller than the potential vorticity depth [i.e., $\xi + f = h(f/H_p) \sim O(\epsilon^{1/3}f)$].

For the case of finite potential vorticity eddies the final calculations must be done numerically. Such calculations were performed for the case where the eddies' relative vorticity at the center varies from $-f_0$ to zero (Fig. 5). The eddy β-induced westward speed was calculated from the formula given by Nof (1981), and the structure of the uniform potential vorticity eddies from the relationships given by Flierl (1979). Also, the main difference between the zero and finite potential vorticity cases is that, in the finite potential vorticity case, both the periodicity and the eddy size are larger than those of the zero potential vorticity.

c. Application

Typical numerical values for the NBC are $Q \approx 45$ Sv, $f_0 \approx 2 \times 10^{-5}\ \mathrm{s}^{-1}$, $g' \approx 2 \times 10^{-2}\ \mathrm{m\ s}^{-2}$, and $\xi/f_0 \approx -0.6$ (where Q is the approaching current transport). The above Coriolis parameter corresponds to a latitude of 8°N, and the above relative vorticity ($\xi/f_0 = -0.6$) corresponds to the observed core of many NBC rings (e.g., see Richardson et al. 1994). For these values, our calculated upstream depth H, Rossby radius R_d, and $\epsilon = \beta R_d/f_0$ are 300 m, 122 km, and 0.122, respectively.

An epsilon of 0.12 corresponds theoretically to a possible error that is greater than 50% because the expansion is done in powers of $\epsilon^{1/6}$. While such a relatively large value for ϵ is certainly not desired, it is in line with other frequently used approximations such as the quasigeostrophic approximation. Despite that the latter approximation is based on a small amplitude expansion, it is routinely applied to eddies and rings whose amplitudes are sometimes even larger than the mean depth (i.e., $\epsilon > 1$). Yet, it frequently gives the correct answer because the components of the neglected terms, which do not contain ϵ, are evidently small. That is to say, perturbation schemes often work even if ϵ is relatively large and it is hard to tell in advance how small ϵ should be.

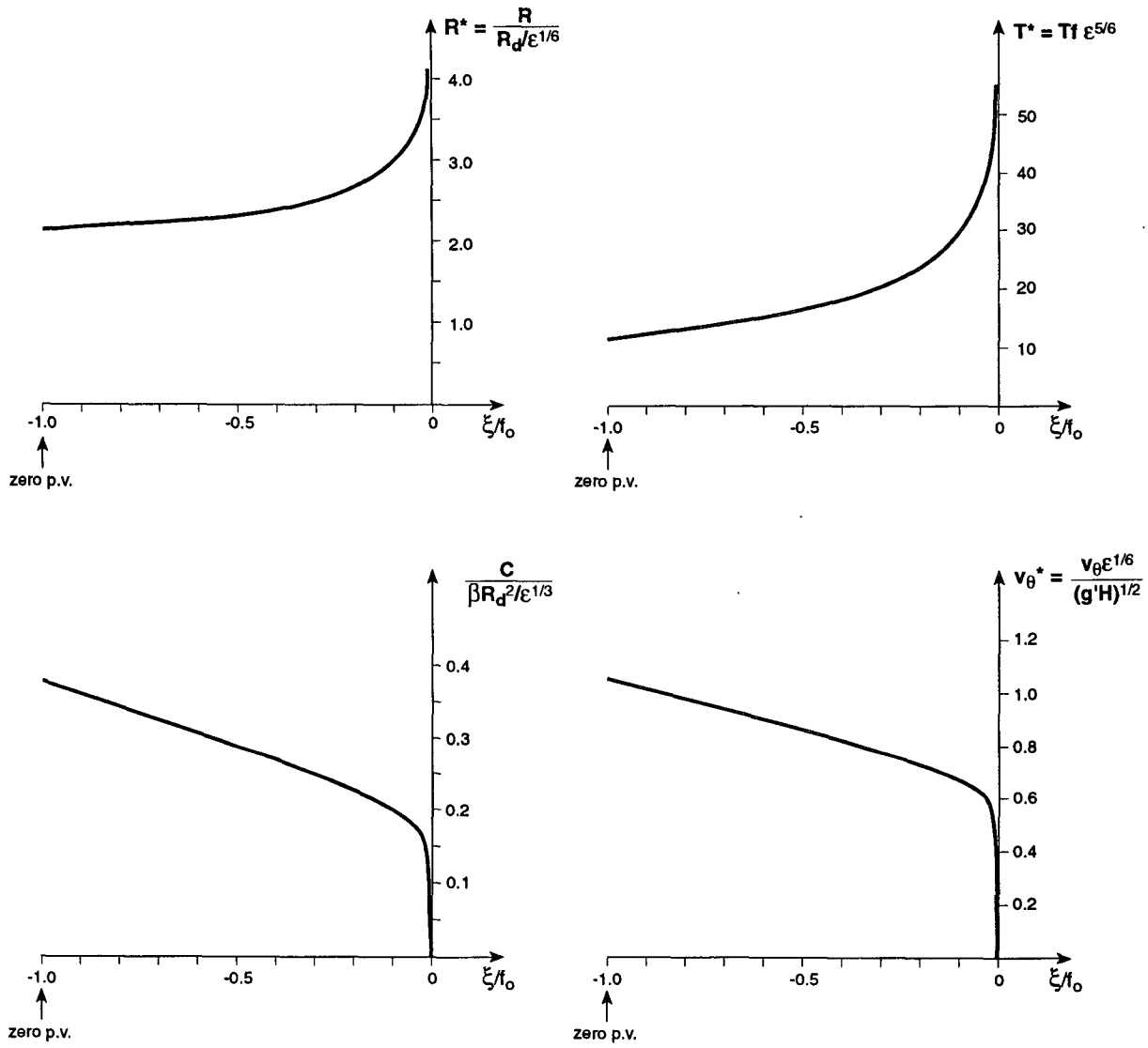

FIG. 5. The eddy radius (R^*), generation period (T^*), drift speed (C^*), and orbital speed along the edge (v_θ^*) as a function of the eddy's relative vorticity (ξ) at the center for the no-topography problem. Zero potential vorticity corresponds to $\xi/f_0 = -1$; all other values correspond to positive uniform potential vorticity.

Our corresponding solution (Fig. 5) indicates that $R^* \approx 2.2$ and $T^* \approx 16$ so that the resulting eddy radius is approximately 380 km and the generation period is roughly 55 days. These reasonable values correspond to a migration rate that is a bit too high [18 cm s^{-1} compared to the observed value of 10 cm s^{-1} or so (Richardson et al. 1994; Fratantoni et al. 1995)] and an eddy volume flux that is also high [21 Sv compared to a temporal average (i.e., an average for the fraction of the year during which the NBC retroflects) of roughly 8 Sv (Fratantoni et al. 1995)]. Although these values are reasonable for a process-oriented study such as ours, a still better estimation can be made by taking into account that the actual migration rate of the eddies is reduced due to the bottom topography. This is consistent with Fratantoni et al.'s (1995) conclusion that NBC rings migrate at half the rate of their open ocean counterparts. The details of the corresponding computations are given in the next section. One may find it peculiar that we are concerned here about a factor of 2 difference in the eddy translation speed and yet overlook similar discrepancies in other properties (such as the eddy depth along their edge). The reason for this is that the migration aspect can be easily corrected, whereas other difficulties cannot be easily ad-

dressed. Also, the newly derived migration formula could be used in other situations where eddies interact with topography and, hence, is worthy of consideration.

6. Solution for the most general case that includes bottom topography

With the aid of the relatively simple solution derived earlier, we shall now derive the more general case where bottom topography slows the propagation of the eddies. The importance of bottom topography can be easily recognized by noting that actual anticyclonic rings in the open ocean tend to propagate toward the southwest due to a combined effect of β and form drag induced by a finite lower layer (absent from a reduced-gravity model). Consequently, the observed northwest migration parallel to the coast indicates that interaction with the topography must be present. Previous attempts to examine the effect of bottom topography on isolated eddies dealt with meridional boundaries (Smith 1986; Smith and O'Brien 1983) where β constantly forces the eddies into the topography. This is quite different from our present case where the β-induced drift and the topographic drift are both acting in the zonal direction.

We shall begin our analysis by deriving a new analytical formula for eddies situated next to a zonal boundary with sloping bottom (Fig. 6).

a. *The propagation of anticyclones due to a combined effect of β and topography*

Consider the lens shown in Fig. 6, and the $\hat{y}$ momentum equation for the outer region S_1 (i.e., the region that is not in contact with the bottom),

$$\hat{u}\frac{\partial \hat{v}}{\partial \hat{x}} + \hat{v}\frac{\partial \hat{v}}{\partial \hat{y}} + (f_0 + \beta\hat{y})(\hat{u} + C) = -g'\frac{\partial h}{\partial \hat{y}}, \quad (6.1)$$

where the origin of our moving coordinate system is now located at the center of the eddy. Here the motions underneath the lens in the region above the topography (i.e., the region bounded by AFED and BFEC) have been neglected. It will become clear later that, due to conservation of potential vorticity, these motions are of the order of $f(\Delta H/H)l \sim O(\beta R_{de}^2)$ so that they are indeed much smaller than the orbital speed of the lens, $f_0 R_{de}$. Consequently, their contribution to the surface integrals, which will be used later, can indeed be neglected.

Multiplication of (6.1) by h, use of the continuity equation and an integration over the area (S_1), and a conversion of the surface integrals to line integrals give

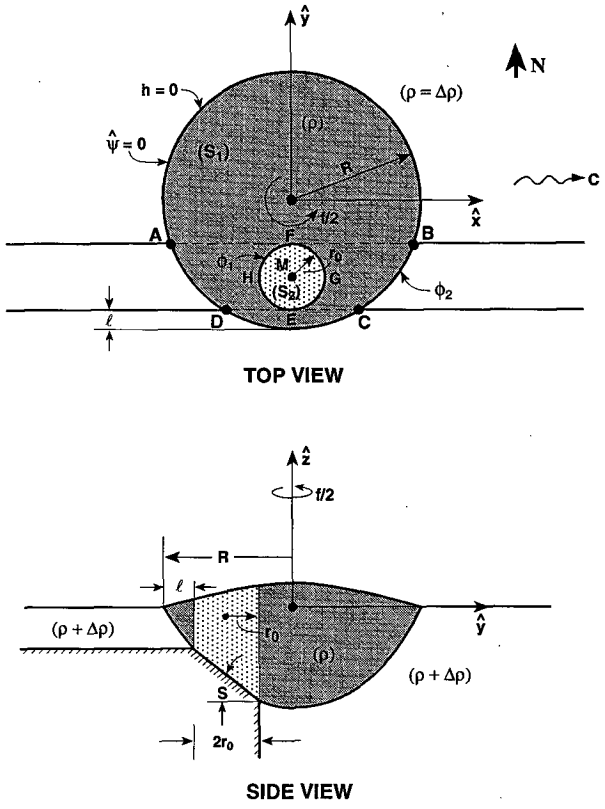

FIG. 6. Schematic diagram of an NBC ring interacting with zonal bottom topography sloping downward toward the north. S_1 is the lens area not in direct contact with the bottom, and S_2 is the region in direct contact with the sloping bottom. We shall see later that $S_2 \sim O[S_1(\beta R_{de}/f_0)^{1/2}]$ and $l \sim O[R(\beta R_{de}/f_0)^{1/4}]$. It is shown in the text that the topography reduces the westward propagation rate.

$$-\oint_{\phi_2} h(\hat{v})^2 d\hat{x} + \oint_{\phi_2} h\hat{u}\hat{v}d\hat{y} + \iint_{S_1} (f_0 + \beta\hat{y})\hat{u}hd\hat{x}d\hat{y} + C\iint_{S_1} fhd\hat{x}d\hat{y} = \frac{g'}{2}\oint_{\phi_2} h^2 d\hat{x}, \quad (6.2)$$

where the first two integrals on the left-hand side and the integral on the right-hand side are performed clockwise around S_2 (i.e., FGEH). It is now further assumed that the topography-induced drift is of the same order as that of β. We shall see shortly that this implies that $S_2 \sim O[S_1(\beta R_{de}/f_0)^{1/2}]$.

The $\hat{y}$ momentum equation for the region in which the lens is in direct contact with the bottom (S_2) is

$$\hat{u}\frac{\partial \hat{v}}{\partial \hat{x}} + \hat{v}\frac{\partial \hat{v}}{\partial \hat{y}} + (f_0 + \beta\hat{y})(\hat{u} + C) = -g\frac{\partial \eta}{\partial \hat{y}}, \quad (6.3)$$

where η is the free surface vertical displacement (measured positively upward). Multiplication of (6.3) by the total depth h, integration over S_2, and conversion to line integrals gives

$$-\oint_{\phi_2} h(\hat{v})^2 d\hat{x} + \oint_{\phi_2} h\hat{u}\hat{v}d\hat{y} + \iint_{S_2} (f_0 + \beta\hat{y})\hat{u}hd\hat{x}d\hat{y} + C\iint_{S_2} fhd\hat{x}d\hat{y}$$
$$= -g\iint_{S_2} h\frac{\partial\eta}{\partial\hat{y}}d\hat{x}d\hat{y} = -g\iint_{S_2}\frac{\partial}{\partial\hat{y}}[h\eta]d\hat{x}d\hat{y} + gS\iint_{S_2}\eta d\hat{x}d\hat{y}, \quad (6.4)$$

where ϕ_2 is the boundary of S_2 and the integration around the boundary is done here in a counterclockwise manner. Across the boundary separating S_2 and S_1, all three variables h, $\hat{u}$, and $\hat{v}$ are continuous and $g\eta = g'h$ because the pressure is continuous. Consequently, the addition of (6.2) and (6.4) gives,

$$\boxed{\beta\iint_{(S_1+S_2)}\hat{\psi}d\hat{x}d\hat{y} + C\iint_{(S_1+S_2)} fhd\hat{x}d\hat{y} = g'\oint_{\phi_2}\frac{h^2}{2}d\hat{x} + gS\iint_{S_2}\eta d\hat{x}d\hat{y},} \quad (6.5)$$

where S is the slope of the bottom [i.e., $[\partial h/\partial y]_M$, where M is the center of S_2 (see Fig. 6)] and the integration around the boundary of S_2 is done in a counterclockwise manner. The two terms on the left-hand side are the familiar β-induced force and the integrated Coriolis force (e.g., see Nof 1981, 1983). The two terms on the right-hand side are the contribution of the sloping bottom to the balance of forces in the N–S direction. The first term is always negative but, as we shall see, is smaller (in absolute value) than the second term, which is always positive. As a result, the topographic effect always reduces the β-induced westward speed. We shall see that, for some range of parameters, this effect causes the eddy to move eastward rather than westward.

To obtain the solution of (6.5), we use a perturbation scheme where the basic state $(\bar{\psi}, \bar{h})$ is associated with an f-plane eddy and the perturbations (C, ψ', h') are associated with the deviations due to the presence of both β and the topography. This gives

$$\beta\iint_{\bar{S}_1}\bar{\psi}d\hat{x}d\hat{y} + C\iint_{\bar{S}_1} f_0\bar{h}d\hat{x}d\hat{y}$$
$$= g'\oint_{(\phi^2)}\frac{\bar{h}^2}{2}d\hat{x} + gS\iint_{\bar{S}_2}\bar{\eta}d\hat{x}d\hat{y}, \quad (6.6)$$

where $\bar{S}_1$ is the area (outside the topography) that the vortex would have on an f plane and $\bar{S}_2$ is the (small) portion of the eddy in direct contact with the bottom. Equation (6.6) can be used for our calculation of the migration rate and, from this point of view, it is not really necessary to proceed further. It is possible to show, however, that it can be simplified considerably. To show this, we convert the first integral on the right-hand side of (6.6) back to a surface integral

$$-g'\iint\bar{h}\frac{\partial\bar{h}}{\partial\hat{y}}d\hat{x}d\hat{y}$$

and expand $\partial\bar{h}/\partial\hat{y}$ in a Taylor series around M, the center of S_2 (see Fig. 6),

$$\frac{\partial\bar{h}}{\partial\hat{y}} = \left[\frac{\partial\bar{h}}{\partial\hat{y}}\right]_M + (\hat{y} + R)\left[\frac{\partial^2\bar{h}}{\partial\hat{y}^2}\right]_M + \cdots, \quad (6.7)$$

where it has been taken into account that the f-plane eddy is symmetric with respect to x. We further recall that, by definition,

$$S \equiv \left[\frac{\partial\bar{h}}{\partial\hat{y}}\right]_M$$

and $g\bar{\eta} = g'\bar{h}$, so that substitution of (6.7) into (6.6) yields

$$\beta\iint_{\bar{S}_1}\bar{\psi}d\hat{x}d\hat{y} + C\iint_{\bar{S}_1} f_0\bar{h}d\hat{x}d\hat{y}$$
$$= -\iint_{\bar{S}_1} f_0\bar{h}(\hat{y} + R)\left[\frac{\partial^2\bar{h}}{\partial\hat{y}^2}\right]_M d\hat{x}d\hat{y}. \quad (6.8)$$

By using a coordinate system located at M (the center of S_2) to evaluate the right-hand side of (6.8) and expanding $\bar{h}$ in a Taylor series around M, the migration formula can be written in a still simpler form,

$$\boxed{C = \left[-\beta\iint_{\text{eddy}}\bar{\psi}dxdy - \frac{g'\pi r_0^4}{4}\left[\frac{\partial\bar{h}}{\partial y}\right]_M\left[\frac{\partial^2\bar{h}}{\partial y^2}\right]_M\right]\Big/ f_0\iint_{\text{eddy}}\bar{h}dxdy,} \quad (6.9)$$

where, as mentioned, $\bar{\psi}$ and $\bar{h}$ are the streamfunction and depth of the corresponding f-plane eddy and the integration is done over the entire eddy (with x and y denoting a coordinate system whose origin is at the

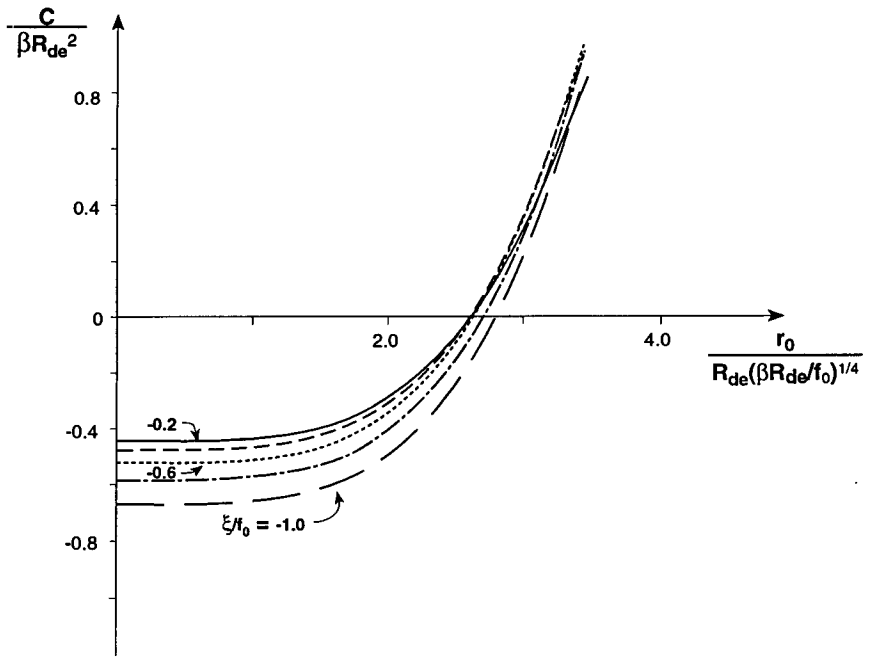

FIG. 7. The combined β and topography-induced migration for a lens adjacent to a zonal boundary with a bottom sloping downward to the north (Fig. 6). R_{de} is the lens Rossby radius, and r_0 is the radius of the area that is in direct contact with the bottom. The shown migration rate is for potential vorticity ranging from zero ($\xi/f_0 = -1.0$) to that corresponding to a relative vorticity of -0.2 at the center of the eddy. Note that for a large enough contact area with the bottom the eddy is translating eastward ($C > 0$) rather than westward ($C < 0$). Also, note that, since the slope S is tangential to the eddy at the center of the contact area, it does not appear explicitly in the figures.

center of the eddy). It is now easy to see that, in order for the terms on the right-hand side of (6.8) to be of the same order as those on the left (so that the topography is as important as β), it is necessary that both r_0 the radius of the contact area S_2 and the penetration distance l be of the order of $R_{de}(\beta R_{de}/f_0)^{1/4}$. Using this scale it is, of course, possible to derive (6.8) with the aid of a formal perturbation expansion. However, due to the different scales in the problem, such a formal derivation is cumbersome; it does not provide any new insights and, therefore, is not presented.

For a zero potential vorticity eddy (6.9) gives the relationship

$$C = -\frac{2}{3}\beta R_{de}^2 + \frac{\sqrt{2}}{128}\left(\frac{r_0}{R_{de}}\right)^4 (g'H_e)^{1/2} + O\left[\beta R_{de}^2\left(\frac{\beta R_{de}}{f_0}\right)\right], \tag{6.10}$$

where the first term is the familiar migration due to β and the second is the contribution of the bottom topography. Recall that, since the slope S and the radius r_0 are related, only one of them appears explicitly in the formula. For a finite potential vorticity corresponding to a core relative vorticity of $-0.6f_0$, the results were found numerically. Together with the results for a zero potential vorticity eddy, they are shown in Fig. 7.

b. Application to NBC rings

When the effect of topography is included, the westward migration rate is reduced. How much it is reduced is not entirely clear as it is not obvious what fraction of the eddy (if any) is in contact with the bottom. However, as mentioned earlier, the fact that NBC eddies are migrating to the northwest (parallel to the coastline) rather than toward the southwest (which is their uninterrupted open ocean propagation pattern) strongly suggests that they interact with the topography. Taking the observed speed of 10 cm s^{-1} to be a result of a speed reduction due to topography, we find from Fig. 7 that $r_0/(\beta R_{de}/f_0)^{1/4}R_{de} \approx 2.5$.

For an NBC transport of 45 Sv such a reduced northwestward speed gives a periodicity of 110 days, a radius of 463 km, and a transport of 16.8 Sv. A reduced speed of 12 cm s^{-1} gives, on the other hand, a somewhat shorter periodicity of 87 days, a smaller radius of 445 km, and a somewhat larger transport of 18 Sv. All of these values are more reasonable than the previous ones, which neglected bottom topography. However, the transport of 16–18 Sv (corresponding to an *an-*

nualized transport of 8–9 Sv), which is about a third of the upstream transport, is still relatively large compared to the observed annualized value of 4 Sv. This is probably a result of our relatively large ϵ ($=0.12$, which corresponds to an error of more than 50% because the expansion is done in powers of $\epsilon^{1/6}$) or a result of the difficulty in identifying the edge of the actual NBC rings.

An additional difficulty is that in all of the above applications, the predicted speeds along the edge of the rings are about 3 m s^{-1}, a value that is obviously too high. This is unavoidable (and typical) for reduced gravity models; it results from the high amplitude along the edge (e.g., see Flierl 1979). Our predicted radii also appear to be large but this is again a result of the reduced gravity model and our use of a lens model for the eddies.

The above results are not very sensitive to the choice of the NBC transport. For instance, with a transport of 25 Sv (instead of the 45 Sv discussed above) and no bottom topography, the radius of the predicted eddies is 340 km (instead of 380 km) and the periodicity is 60 days (instead of 55 days). (The corresponding values for the undisturbed depth, Rossby radius, and epsilon are 225 m, 106 km, and 0.11.) With bottom topography that causes a migration rate of 10 cm s^{-1}, the predicted radius is 385 km and the periodicity is 71 days.

7. Conclusions

The aim of our theory was to examine a new eddy generation mechanism that is related to the flow force of a retroflecting current. The new inviscid generation process is similar to that associated with a flow from a channel, which was termed by PNa "the momentum imbalance paradox" and to that of a current around a cape (PNb.) It implies that a light retroflecting current (Fig. 2) exerts a flow force (parallel to the wall) that cannot be balanced without the generation of eddies on the opposing side (Fig. 3). For the eddies to be generated periodically, it is necessary that there be an agent responsible for their removal from the generation area. This is provided by β, which carries the eddies toward the west.

Using an integrated momentum technique that involves nonlinear time-dependent processes, we have computed the structure of the resulting eddies and their generation frequency (Fig. 5). As in PNa,b, a retroflection length scale for eddies emerges from our calculations. In contrast to most eddies whose length scale is equal to the Rossby radius of the parent current (R_d), the eddies have a length scale of $R_d/\epsilon^{1/6}$ where $\epsilon = \beta R_d/f_0$) and, hence, are somewhat larger than most eddies.

For values typical for the NBC (e.g., a flux of 45 Sv and a latitude of 8°N), the above model predicts that rings will be produced every 50 days or so, that they will migrate at 18 cm s^{-1}, and that they will transport more than 20 Sv (during the period that the NBC retroflects). Although these values are reasonable, both the migration speed and the transport are somewhat too high. Better values can be obtained if one takes into account that the sloping bottom topography (Fig. 6) reduces the westward migration rate to 10 or 12 cm s^{-1}. A fair portion of the discussion has been devoted to this aspect and a new eddy migration formula has been derived (6.9, 6.10). The reduced migration rate corresponds to a much more realistic generation frequency of 90 days or so and a slightly more realistic transport of 16–18 Sv (corresponding to an annualized transport of 8–9 Sv), which is about a third of the upstream transport of 45 Sv. It should be kept in mind, however, that our primary purpose is to point out a new nonlinear eddy-generation process rather than quantitatively reproduce all the observed features. As such, the model is very useful.

Acknowledgments. This study was supported by the National Science Foundation under Contracts OCE 9012114 and OCE 9102025 and Office of Naval Research Grant N00014-89-J-1606. T. Pichevin was funded by Service Hydrographique et Océanographique de la Marine (SHOM) and Direction des Recherches, Etudes et Techniques (DRET). Two anonymous reviewers provided penetrating and helpful comments. Computations were carefully checked by Steve Van Gorder. Drawings and typing were done by Beth Raynor.

APPENDIX

List of Symbols

a	eddy width along the $\hat{x}$ axis
b_1, b_2	distances between the eddy edges and the coast (Fig. 3)
b_1^*, b_2^*	nondimensional distances between the eddy edges and the coast
C	eddy migration rate
f	Coriolis parameter ($f_0 + \beta y$)
g'	"reduced gravity" $(\Delta\rho/\rho)g$
$\underline{h}$	thickness of light water
$\bar{h}$	dimensional depth of an f-plane eddy
H	upstream undisturbed current depth
l	distance between the eddy's edge and the edge of the region that is in direct contact with the bottom
L	longshore current width
M	center of S_2
r, θ	polar coordinates
R	eddy diameter
R_d	Rossby radius of the parent current
R_{de}	Rossby deformation radius of the eddy
S	integration area
S_1	portion of the eddy that is not in contact with the bottom

S_2	portion of the eddy that is in contact with the bottom
T	period of eddy generation
u, v	velocities in Cartesian coordinates
v_θ	orbital velocity
$\hat{x}, \hat{y}, \hat{t}$	moving coordinates system
$x_e^*, y_e^*, u_e^*, v_e^*, h_e^*$	scaled variables associated with the eddies on the left
α	unknown of order unity that measures the size of the resulting eddies
ϵ	small parameter equal to $\beta R_d/f_0$
ϕ	boundary of integration area S
γ	the inclination of the coastline
μ	small parameter equal to $\beta R_{de}/f_0$
$\rho, \Delta\rho$	density and density difference between the layers
ψ	steady streamfunction (defined by $\partial\psi/\partial y = -uh$; $\partial\psi/\partial x = vh$)
$\hat{\psi}$	streamfunction in the moving coordinate system
$\tilde{\psi}$	time-integrated streamfunction
$\underline{\psi}$	streamfunction of a steady f-plane eddy
ξ	relative vorticity
$\oint$	clockwise integration
$\oint$	counterclockwise integration

REFERENCES

Brown, W. S., W. E. Johns, K. D. Leaman, J. P. McCreary, R. L. Molinari, P. L. Richardson, and C. Rooth, 1992: A western tropical Atlantic experiment (WESTRAX). *Oceanography,* **5,** 73–77.

Bruce, J. G., 1984: Comparison of eddies off the North Brazilian and Somali coasts. *J. Phys. Oceanogr.,* **14,** 825–832.

——, and J. L. Kerling, 1984: Near equatorial eddies in the North Atlantic. *Geophys. Res. Lett.,* **11,** 779–782.

——, ——, and W. H. Beatty III, 1985: On the North Brazilian eddy field. *Progress in Oceanography,* Vol. 14, Pergamon, 57–63.

Bryden, H., and M. Hall, 1980: Heat transport by currents across 25°N latitude in the Atlantic Ocean. *Science,* **207,** 884–886.

Cochrane, J. D., F. J. Kelly, and C. R. Olling, 1979: Subthermocline countercurrents in the western equatorial Atlantic Ocean. *J. Phys. Oceanogr.,* **9,** 724–738.

Condie, S. A., 1991: Separation and recirculation of the North Brazil Current. *J. Mar. Res.,* **49,** 1–19.

Csanady, G. T., 1985: A zero potential vorticity model of the North Brazilian Coastal Current. *J. Mar. Res.,* **43,** 553–579.

——, 1990: Retroflection and leakage in the North Brazil Current: Critical point analysis. *J. Mar. Res.,* **48,** 701–728.

Didden, N., and F. Schott, 1993: Eddies in the North Brazil Current retroflection region observed by Geostat altimetry. *J. Geophys. Res.,* **98,** 20 121–20 131.

Flierl, G., 1979: A simple model of the structure of warm and cold-core rings. *J. Geophys. Res.,* **84,** 78–85.

Fratantoni, D., W. E. Johns, and T. L. Townsend, 1995: Rings of the North Brazil Current: Their structure and behavior inferred from observations and a numerical simulation. *J. Geophys. Res.,* **100**(C6), 10 633–10 654.

Holland, W. R., and F. Bryan, 1987: Progress in the WOCE Ocean Community Modeling Effort (abstract). *Eos, Trans. Amer. Geophys. Union,* **68,** 1311.

Hurlburt, H. E., and J. D. Thompson, 1980: A numerical study of Loop Current intrusions and eddy shedding. *J. Phys. Oceanogr.,* **10,** 1611–1651.

Johns, W. E., T. N. Lee, and F. A. Schott, 1990: The North Brazil Current retroflections: Seasonal structure and eddy variability. *J. Geophys. Res.,* **95,** 22 103–22 120.

Metcalf, W., and M. Stalcup, 1967: Origins of the Atlantic Equatorial Undercurrent. *J. Geophys. Res.,* **72,** 4959–4975.

Nof, D., 1981: On the β-induced movement of isolated baroclinic eddies. *J. Phys. Oceanogr.,* **11,** 1662–1672.

——, 1983: On the migration of isolated eddies with application to Gulf Stream rings. *J. Mar. Res.,* **41,** 399–425.

Ou, H. W., and W. P. M. De Ruijter, 1986: Separation of an inertial boundary current from a curved coastline. *J. Phys. Oceanogr.,* **16,** 280–289.

Philander, S. G., and R. Pacanowski, 1986: A model of the seasonal cycle in the tropical Atlantic Ocean. *J. Geophys. Res.,* **91,** 14 192–14 206.

Pichevin, T., and D. Nof, 1996a: The momentum imbalance paradox. *Tellus,* in press.

——, and ——, 1996b: The eddy cannon. *Deep-Sea Res.,* in press.

Richardson, P. L., G. E. Hufford, R. Limeburner, and W. S. Brown, 1994: North Brazil Current retroflection eddies. *J. Geophys. Res.,* **99,** 5081–5093.

Rintoul, S. R., 1991: South Atlantic interbasin exchange. *J. Geophys. Res.,* **96,** 2675–2592.

Schott, F. A., and C. W. Boning, 1991: The WOCE model in the western equatorial Atlantic: Upper layer circulation. *J. Geophys. Res.,* **96,** 6993–7004.

Smith, D. C., IV, 1986: A numerical study of loop current eddy interaction with topography in the western Gulf of Mexico. *J. Phys. Oceanogr.,* **16,** 1260–1272.

——, and J. J. O'Brien, 1983: The interaction of a two-layer isolated mesoscale eddy with bottom topography. *J. Phys. Oceanogr.,* **13,** 1681–1697.